ACS APPLIED MATERIALS & INTERFACES

Research Article

www.acsami.org

Surface Immobilization of a Tetra-Ruthenium Substituted Polyoxometalate Water Oxidation Catalyst Through the Employment of Conducting Polypyrrole and the Layer-by-Layer (LBL) Technique

Nargis Anwar,[†] Andrea Sartorel,[‡] Mustansara Yaqub,[†] Kevin Wearen,[†] Fathima Laffir,[§] Gordon Armstrong,[§] Calum Dickinson,[§] Marcella Bonchio,[‡] and Timothy McCormac*[,†]

[†]Electrochemistry Research Group, Department of Applied Science, Dundalk Institute of Technology, Dublin Road, Dundalk, County Louth, Ireland

[‡]ITM-CNR and Department of Chemical Science, University of Padova, via Marzolo 1, 35131 Padova, Italy

[§]Materials and Surface Science Institute, University of Limerick, Limerick, Ireland

Supporting Information

ABSTRACT: A tetra Ru-substituted polyoxometalate $Na_{10}[\{Ru_4O_4(OH)_2(H_2O)_4\}(\gamma\text{-}SiW_{10}O_{36})_2]$ (Ru_4POM) has been successfully immobilised onto glassy carbon electrodes and indium tin oxide (ITO) coated glass slides through the employment of a conducting polypyrrole matrix and the layer-by-layer (LBL) technique. The resulting Ru_4POM doped polypyrrole films showed stable redox behavior associated with the Ru centres within the Ru_4POM, whereas, the POM's tungsten-oxo redox centres were not accessible. The films showed pH dependent redox behavior within the pH range 2−5 whilst exhibiting excellent stability towards redox cycling. The layer-by-layer assembly was constructed onto poly(diallyldimethylammonium chloride) (PDDA) modified carbon electrodes by alternate depositions of Ru_4POM and a Ru(II) metallodendrimer. The resulting Ru_4POM assemblies showed stable redox behavior for the redox processes associated with Ru_4POM in the pH range 2−5. The charge transfer resistance of the LBL films was calculated through AC-Impedance. Surface characterization of both the polymer and LBL Ru_4POM films was carried out using atomic force microscopy (AFM), X-ray photoelectron spectroscopy (XPS), and scanning electron microscopy (SEM). Initial investigations into the ability of the Ru_4POM LBL films to electrocatalytically oxidise water at pH 7 have also been conducted.

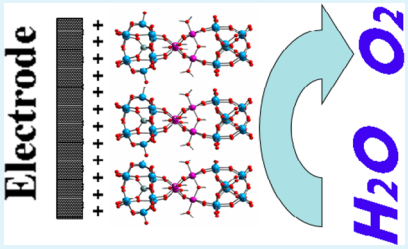

KEYWORDS: *polyoxometalates, immobilization, conducting polymer, water oxidation, multilayer assembly, electrocatalysis*

INTRODUCTION

Replacing fossil fuels by splitting water to produce hydrogen and oxygen is a key objective for alternative energy applications.[1−5] The splitting of water, shown in eq 1 is endoergonic by 4.92 eV,[6] with significant kinetic barriers, primarily due to the multi-electronic nature of the two redox reactions involved (eqs 2 and 3):

$$2H_2O \rightarrow 2H_2 + O_2 \quad (1)$$

$$2H_2O \rightarrow 4H^+ + 4e^- + O_2 \quad (2)$$

$$4H^+ + 4e^- \rightarrow 2H_2 \quad (3)$$

In particular, oxidizing water to oxygen (eq 2) is the most difficult step to achieve. The mechanism involves exchange of four electrons and four protons, and formation of a new O−O bond, requiring the use of a catalyst. In nature, photosynthesis provides a very good model for the oxidation of water. The electrons required for photosynthesis to occur are obtained from water by Photosystem II, an oxygen-evolving protein complex (OEC), and its structure was recently resolved at 1.8 Å resolution.[7] It consists of four manganese atoms and one calcium atom, which are connected to each other through oxo-bridges. Five redox states are involved in this tetra-electronic process.[8−11] The first synthetic molecular catalyst resembling OEC was prepared a few decades ago named as "blue dimer", $[(bpy)_2(H_2O)Ru(III)(\gamma\text{-}O)Ru(III)(H_2O)(bpy)_2]^{4+}$, (bpy = 2,2′-bipyridine).[12] This blue dimer operated electrochemically or in the presence of a strong oxidizer such as Ce(IV) resulting in the loss of $4e^-$ / $4H^+$ so as to produce an intermediate capable of oxidizing water.[12−14] The stability of this "blue dimer" was still a challenge, but it opened up a new way to produce more synthetic catalysts for water oxidation. The majority of synthetic molecular catalyst analogues of OEC are based on ruthenium.[15−23] W, V, Mo, Nb, and Ta in their highest oxidation states are capable of making metal-oxide cluster anions, generally referred to as polyoxoanions or polyoxometalates (POMs).[24] Their diverse molecular and electronic structures ensure they are employed across a wide range of applications from molecular electronics to catalysis.[25−28] Combining the properties of a POM and ruthenium

Received: November 22, 2013
Accepted: April 23, 2014
Published: April 23, 2014

   dx.doi.org/10.1021/am405295c | ACS Appl. Mater. Interfaces 2014, 6, 8022−8031

yielded a fully inorganic water splitting catalyst.[23,29−31] The electrochemical water oxidation by the Ru_4POM has already been reported both in solution and when supported in nanostructured materials.[30,32−35,38] For this catalyst, four Ru(IV) centres are stabilised between two POM units through the presence of oxo/hydroxo ligands.[5,23,29,32,35−37] Figure 1

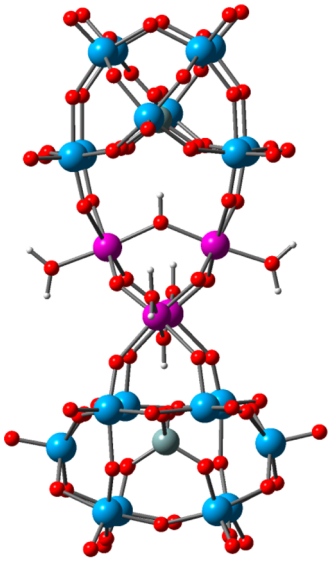

Figure 1. Structural demonstration of Ru_4POM, showing the ball and stick model where Ru (purple), O (red), H (gray), W (blue), and Si (bluish green) are presented.

shows the ball and stick structural model of $\{Ru_4(\mu\text{-}O)_4(\mu\text{-}OH)_2(H_2O)_4[\gamma\text{-}SiW_{10}O_{36}]_2\}$, which consists of two twisted dimeric structures with two γ-SiW_{10} units. These two units are connected to the electrophilic central core $[Ru_4(\mu\text{-}O)_4(\mu\text{-}OH)_2(H_2O)_4]^{6+}$ in a 90° staggered arrangement. The symmetry of the overall polyanion is D_{2d}. The four ruthenium atoms are at the apexes of a tetrahedron whereas the six oxygen atoms are at the apexes of an octahedron. Two oxygen atoms within the $Ru_4O_4^{6+}$ core are monoprotonated. These two protonated oxygen atoms bend and join the two adjacent Ru(IV) atoms, which are connected to the binding sites of the POM. The ruthenium centres of different monomeric centres are bridged by the oxo-ligands.[23] This has been demonstrated to be a very stable and efficient catalyst for the electrocatalytic[33,34,38] and chemical[31] based splitting of water; its efficiency is comparable to other well developed molecular catalysts.[27,28,39−41]

Immobilization of POMs onto electrode surfaces can improve their electrochemical stability and aid in their applications in the field of electrocatalysis.[42,43] Besides developing new water oxidation catalysts, a major issue deals with their immobilization onto electrodes, to achieve heterogeneous catalysis maintaining their inherent solution activity. Ru_4POM has been successfully supported onto multiwalled carbon nanotubes exploiting electrostatic interactions with positively charged pendant arms anchored to the tube surface.[44] In another approach, the Ru_4POM was immobilized through the layer-by-layer self-assembly technique with polyethylenimine. The resulting LBL assembly showed good stability but the system was not investigated for water oxidation.[45] In this work, the immobilization of the Ru_4POM was carried out to produce a solid state electrocatalyst for water oxidation. Glassy carbon electrode surfaces and ITO coated glass slides have been used to incorporate the Ru_4POM into conducting polypyrrole and through the employment of the layer-by-layer assembly technique with a Ru(II)-metallodendrimer $[RuDend]^{8+}$ (Supporting Information Figure S1) as the cationic moiety within the LBL assembly. It is worth noting that since the Ru-metallodendrimer is photoactive, in principle, this approach could be applied to design a photoanode for water oxidation, by constructing the layer-by-layer assembly onto a semiconducting electrode surface. In addition, the electrocatalytic oxidation of water has been tested in pH7 PBS buffer using Ru_4POM and Ru(II)-metallodendrimer assembly.

2. EXPERIMENTAL SECTION

2.1. Materials. The sandwich type $[\{Ru_4O_4(OH)_2(H_2O)_4\}(\gamma\text{-}SiW_{10}O_{36})_2]^{10-}$ (Ru_4POM) and the pentaerythritol based Ru-metallodendrimer $[RuDend]^{8+}$ were prepared as previously reported.[23,46] All other chemicals were purchased from Aldrich, were of reagent grade, and were used as received. An 8% v/v solution of MW 20 000 poly(diallyldimethylammonium chloride) (PDDA) was prepared from stock as received. Pyrrole (C_4H_5N, 99%) was received from ACROS Organics and purified before use by passing through a neutral Al_2O_3 column to obtain a colourless liquid. Alumina electrode polishing powders of different sizes (0.05, 0.3, and 1.0 μm) were purchased from CH Instruments. Purified water was obtained using a Milli-Q water purification system.

2.2. Apparatus and Procedures. Electrochemical experiments were performed in a conventional three electrode electrochemical cell using a CHI660 electrochemical workstation. A glassy carbon electrode (GCE) 3 mm diameter was used as the working electrode, a platinum wire as the counter electrode, and an aqueous Ag/AgCl (3 M KCl) as the reference electrode unless otherwise stated. Alumina powders were used for the cleaning of the working electrode and the polishing sequence was 1.0, 0.3, and 0.05 μm Al_2O_3. The electrode was thoroughly rinsed after each polishing step with deionized water, rinsed with ethanol at the end of the polishing process and dried with a high purity nitrogen gas stream. All solutions were degassed for 20 min prior to the electrochemical experiments with high purity nitrogen gas so as to remove any dissolved oxygen. Electrolytes used to prepare the buffer solutions were 1 M LiCl (pH 2, 2.5) and 1 M $LiCH_3COO$ (pH 3, 3.5, 4, 4.5, 5) with the pH being adjusted with either 1 M HCl or 1 M CH_3COOH as appropriate. Phosphate buffered saline [PBS] pH 7 was used for the electrocatalytic oxidation of water investigations. 10 mM solutions of potassium ferricyanide and potassium ferrocyanide in 0.1 M potassium chloride solution were used for electrochemical impedence spectroscopy (EIS). The recording of the spectra were performed at an applied potential of +230 mV (versus Ag/AgCl) from 0.1 to 1×10^6 Hz with a voltage amplitude of 5 mV. The working electrode was rinsed thoroughly in deionized water before and after each recording and was dried with high purity nitrogen gas. The electrolyte was freshly prepared before use and was stored in the dark.

Scanning electron microscopy (SEM) of the Ru_4POM doped polymer films was performed on a Hitachi SU-70 FESEM using accelerating voltages of 3 kV and 20 kV. Films were uncoated as a low voltage (3 kV) was employed to avoid charging effects during imaging. Energy dispersive spectroscopy (EDS) used an Oxford Instruments SDD X-max detector with 50 mm^2 window and operated at accelerating voltage of 20 kV.

X-ray photoelectron spectroscopy (XPS) analysis of the Ru_4POM based multilayers and polymer films was performed by a Kratos AXIS 165 spectrometer using monochromatic Al Kα radiation of energy 1486.6 eV. 160 and 20 eV pass energies were used for survey spectra and narrow regions, respectively. The atomic concentrations of the chemical elements were investigated in the near-surface region after subtraction of a Shirley type background by considering the corresponding Scofield atomic sensitivity factors. The low energy electrons were flooded to efficiently neutralize the sample surface.

Core level binding energies were determined using C 1s peak at 284.8 eV as the charge reference.

Atomic force microscopy (AFM) was conducted in AC ("tapping") mode on an Agilent 5500 instrument controlled using PicoView 1.10.1 software. Micromasch NSC15 cantilevers (tetrahedral tips, radius < 10 nm, resonant frequency ~ 325 kHz) and Micromasch NSC14 cantilevers (as NSC15 with resonant frequency ~ 160 kHz) were used to image the Ru_4POM LBL and polymer films, respectively. The image sizes used for each sample were chosen based on the expected dimensions of the features of interest identified from SEM analysis. Multiple regions were imaged on each sample; representative images are presented here. Scan conditions were optimized to suit the features observed for each sample. All images presented were obtained at 512 pixel resolution. Image analysis was undertaken using PicoImage Advanced 5.1.1 software. The raw topography and amplitude data was leveled, noise was removed by applying a spatial filter, and line noise arising from artifacts was removed where necessary. S_q, the root mean squared height of the features observed for each sample, was determined according to ISO 25178. The resulting topography profiles are presented as pseudo-colour images.

Raman spectra were acquired with a Renishaw instrument, model Invia reflex equipped with 532, 633, and 785 nm lasers.

2.3. Ru_4POM Doped Polypyrrole Formation. The method described in the literature[47] was employed with minor modifications for the electrochemical surface immobilization of the Ru_4POM doped polypyrrole films. Polypyrrole films were grown by either employing the sodium or tetrabutylammonium salt of the Ru_4POM from aqueous or acetonitrile solutions, respectively. Films of varying surface coverage were grown at a constant potential of +0.65 V with different deposition charges of 1, 5, and 10 mC from a solution containing 0.1 M pyrrole monomer and 0.001 M Ru_4POM. After formation the polymer modified electrode was washed with 0.1 M HCl solution.

2.4. Construction of Multilayer Assemblies of Ru_4POM and RuDend. The procedure followed for the construction of multilayer assembly of Ru_4POM and $[RuDend]^{8+}$ onto glassy carbon electrode surfaces and indium−tin oxide coated glass slides was reported by our group previously.[48] Schematic representation of the LBL assembly is shown in Supporting Information Figure S2. A glassy carbon electrode was first dipped for 60 min in 8% v/v aqueous PDDA solution. The electrode was rinsed thoroughly with de-ionized water and dried with nitrogen gas. The electrode was then immersed for 20 min in a 3.4 mM Ru_4POM acetonitrile solution. After deposition of the POM layer the electrode was then dipped in a 0.2 mM Ru-metallodendrimer acetonitrile solution for 20 min. The electrode was then rinsed after every dipping step with acetonitrile. In this way, one bilayer was constructed and the steps were then repeated so as to construct the desired number of bilayers within the assembly. Cyclic voltammograms were recorded in 0.1 M HCl after the deposition of each POM layer during the LBL construction procedure.

3. RESULTS AND DISCUSSION

3.1. Redox Properties of $Na_{10}[\{Ru_4O_4(OH)_2(H_2O)_4\}(\gamma\text{-}SiW_{10}O_{36})_2]$ in Solution. Figure 2 represents the cyclic voltammogram of 1 mM Ru_4POM in 0.1 M HCl. The presence of five clear mono-electronic redox couples, with formal potentials, $E_{1/2}$ of +0.226 V, +0.473, +0.636, +0.893, and +1.064 (vs Ag/AgCl) is readily apparent. These correspond to the POM's Ru based redox processes with the identity of the redox states involved having been debated in the literature,[35−37] with the five waves being attributed to Ru(IV)/(III), Ru(V)/(IV), Ru(V)/(IV), Ru(V)/(IV), and Ru(V)/(IV) couples[36] or more recently to Ru(IV)/(III), Ru(IV)/(III), Ru(IV)/(III), Ru(V)/(IV), and Ru(V)/(IV) couples, by taking advantage of a combination of data derived from dc cyclic, rotating disk electrode, and Fourier transform large amplitude ac voltammetry.[35,37] This debate falls beyond the aims of the present work, where these ruthenium-based waves are used as a probe of anchoring the title compound onto different surfaces.

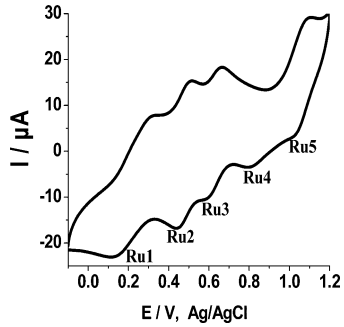

Figure 2. Redox activity of Ru_4POM in solution. Cyclic voltammogram was recorded at GCE in 1 mM solution of Ru_4POM in 0.1 M HCl at a scan rate of 50 mV/s.

Therefore, the five redox waves are herein identified as Ru1, Ru2, Ru3, Ru4, and Ru5, respectively. In absence of KNO_3, the two waves Ru1 and Ru2 are not resolved, as reported.[30] Furthermore, one bielectronic and one four electron wave were also observed with the values of $E_{1/2}$ −256 and −455 mV (vs Ag/AgCl), respectively, with these corresponding to the redox activity of the POM's W−O framework and indicated as W1 and W2.

3.2. Surface Immobilization of $[\{Ru_4O_4(OH)_2(H_2O)_4\}(\gamma\text{-}SiW_{10}O_{36})_2]^{10-}$. *3.2.1. Ru_4POM Doped Polypyrrole Films.* Conducting polymeric films based on Ru_4POM and polypyrrole were fabricated onto the GCE and ITO coated glass slides in aqueous and organic media. Films were deposited with deposition charges of 1, 5, and 10 mC. Figure 3A is the resulting cyclic voltammogram of a Ru_4POM doped polypyrrole film, grown from acetonitrile, of surface coverage 1.7×10^{-10} mol cm^{-2} in 0.1 M HCl. The three well-defined monoelectronic waves Ru3, Ru2, and Ru1 are readily observed. The $E_{1/2}$ values of these couples are +606, +460, and +263 mV (vs Ag/AgCl). These values are in good agreement with the solution phase values obtained for the same processes. However, in the polypyrrole matrix the Ru1 wave appears as two separate waves (Ru0 and Ru1), similarly to what happens in solution when 1 M KNO_3 is used as the supporting electrolyte.[30]

The ΔE values for these redox processes are 7, 5, and 12 mV (vs Ag/AgCl), respectively, representing close to ideal thin layer behavior. Scanning the electrode potential further negative, so as to view the Ru_4POM's tungsten-oxo redox processes proved unsuccessful.

Thin layer behavior for the film was observed up to scan rates of 1000 mV/s, whereas for thicker films, with surface coverages of 6.6×10^{-10} mol cm^{-2}, thin layer behavior was observed up to scan rates of 500 mV/s. Table 1 summarizes the redox behavior of Ru_4POM doped polypyrrole films, of varying surface coverage, as a function of scan rate. The values of the peak to peak separations are very near to the theoretical zero value. The anodic and cathodic full width at half maximum (FWHM) values can be seen to be close to the expected theoretical value of 90.6 mV for thinner films at slower scan rates. A Ru_4POM doped polypyrrole film, with a surface coverage of 2.1×10^{-10} mol cm^{-2}, showed relatively good stability towards redox switching, with the percentage loss of global redox activity being 16, 18, and 21% for the 25th, 49th, and 100th redox cycles, respectively (Supporting Information Figure S4). As expected, the three Ru redox processes associated with the Ru_4POM moiety within the polypyrrole film showed pH

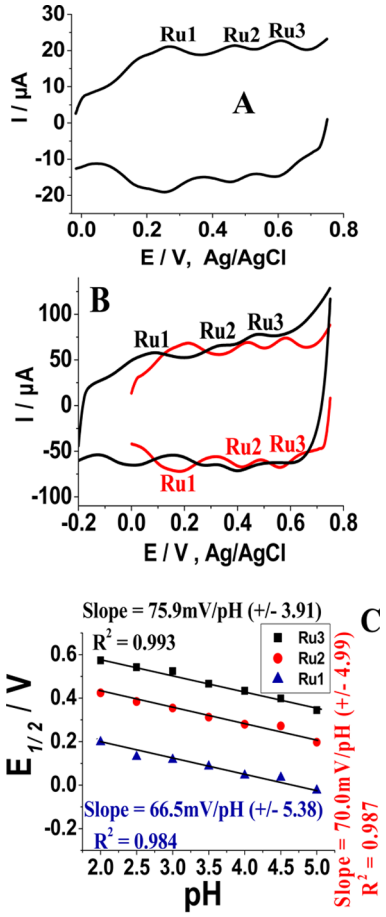

Figure 3. (A) Cyclic voltammograms of Ru_4POM entrapped into polypyrrole film of surface coverage 1.68×10^{-10} mol cm^{-2} in 0.1 M HCl at scan rate 50 mV/s. (B) pH dependence of Ru_4POM doped polypyrrole film in pH2 (red) and pH 4 (black) scan rate 50 mV/s. (C) Dependence of the observed formal potential on to the pH.

dependent behavior in the pH range 2 to 5 as observed in Figure 3B. It is seen that as the pH was made more alkaline the Ru redox processes shifted cathodically with the number of protons associated with each redox process being calculated from the dependencies of the formal potentials upon the solution pH as shown in Figure 3C. The resulting slope values for the Ru1, Ru2, and Ru3 redox processes plots are 66(±5), 70(±5), and 76(±4) mV per decade change in pH, respectively, thereby indicating the addition of one proton per monoelectronic redox process, as observed in solution.[35] The importance of "proton coupled electron transfer" (PCET) events in water oxidation catalysis is well recognized,[49] since they allow "potential leveling of subsequent redox couples"[50] thus allowing catalysis to occur at lower over-potentials. Leveling of redox potentials in subsequent PCET events is mainly attributed to the absence of a net charge variation in the catalyst, since removal of negative charged electrons is compensated by contemporary loss of positively charged protons. Therefore, the presence of several PCET events in the Ru_4POM moiety is a further confirmation of the extraordinary ability of this molecule to catalyse water oxidation at low over-potentials.[50]

However, it was recently reported that proton transfer may not be necessarily coupled to all electron transfer steps that generate water oxidizing intermediate forms of Ru_4POM, and that alkali and earth alkali cations, in particular K^+, may compete with H^+ in interactions with the POM.[30] Ru_4POM doped polymeric films grown from aqueous and organic media exhibited similar electrochemical behavior as is indicated in Supporting Information Figure S3. In addition to the electrochemical responses the identity of the Ru_4POM in the polymer matrix was confirmed by the resonant Raman signals between 250 and 500 cm^{-1} (Supporting Information Figure S9.

3.2.2. Ru_4POM–[RuDend]$^{8+}$ LBL Films. Multilayer assemblies based upon the anionic Ru_4POM and cationic $[RuDend]^{8+}$ moieties were fabricated onto PDDA modified GCE and ITO coated glass slides by using the procedure detailed in the Experimental section. Growth of the LBL assembly was monitored by recording the cyclic voltammograms of the resulting layers in 0.1 M HCl after the deposition of each Ru_4POM layer. Figure 4B exhibits the resulting cyclic voltammograms during the deposition of the LBL assembly consisting of 7 Ru_4POM monolayers with an outer Ru_4POM layer. As seen in Figure 4B during the construction, only three clear redox processes are observed, these are believed to be the Ru1, Ru2, Ru3 processes with the more positive Ru4 and Ru5 couples overlapping in potential to the metallodendrimer's Ru(III)/(II) redox process. Table 2 shows the electrochemical parameters of both the Ru_4POM in solution and as the first monolayer upon a PDDA modified GCE (as shown in Figure 4A).

It can be seen that the values of formal potentials of all the Ru-centers within the POM in solution and within the layer are

Table 1. Electrochemical Redox Properties of PPy-Ru_4POM Hybrid Films As a Function of Surface Coverage and Scan Rate at GCE in 0.1 M HCl (vs Ag/AgCl) for the Ru2 Wave

Γ (mol cm^{-2}) × 10^{-10}	scan rate (mV/s)	E_{pa} (mV)	E_{pc} (mV)	$E_f^{o\prime}$ (mV)	ΔE_p (mV)	FWHM anodic (mV)	FWHM cathodic (mV)
	5	+462	+450	+456	12	96	82
	10	+462	+456	+459	6	98	76
1.68	50	+462	+458	+460	4	76	68
	100	+465	+457	+461	8	78	70
	5	+485	+488	+486	3	76	84
	10	+488	+487	+487	1	84	72
2.14	50	+491	+486	+488	5	84	74
	100	+494	+485	+489	9	84	-72
	5	+440	+442	+441	2	94	80
	10	+449	+452	+450	3	86	72
6.64	50	+461	+452	+456	9	84	72
	100	+466	+450	+458	16	80	72

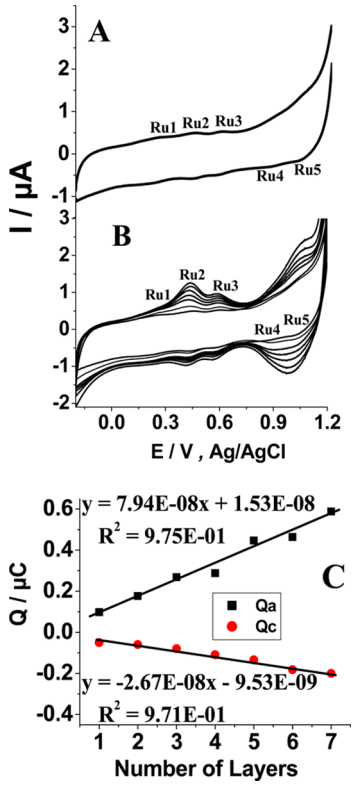

Figure 4. (A) Cyclic voltammograms of a monolayer film composed Ru_4POM. (B) Cyclic voltammograms of a multilayer film composed of 6 bilayers Ru_4POM-RuDend with an outer anionic layer in 0.1 M HCl solution at a GCE. Scan rate was 50 mV/s. (C) The dependences of peak charges of Ru2 redox process on the number of layers.

comparable; the W−O redox process of the POM was not recorded during the construction. Unlike the polymeric films, however, the W−O processes were accessible with a formal potential of −426 and −553 mV for 1st and 2nd bi- and tetra-electronic W−O processes, respectively. These formal potential were more negative as compared to the solution phase values of these processes, possibly because of the interactions of the anionic and cationic species within the LBL assembly. The resulting assembly was reproducible from layer to layer and sample to sample. The constructed assembly exhibits a continuous growth in the surface coverage from 0.01 nmol cm^{-2} for the 1st Ru_4POM layer to 0.1 nmol cm^{-2} for the 7th Ru_4POM layer calculated from the integration of the Ru2 wave. Continuous increase in the deposition charge associated with the anodic and cathodic peaks of the Ru2 redox process versus the layer number is shown in Figure 4C.

Cyclic voltammograms obtained as a function of scan rate are shown in Figure 5A. Figure 5B shows the associated peak

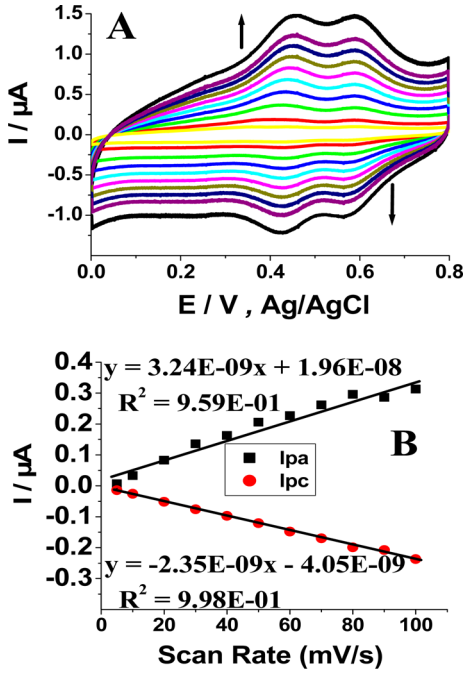

Figure 5. (A) Cyclic voltammograms of a multilayer film of 6 bilayers of Ru_4POM-RuDend in 0.1M HCl solution scan rates 5 (innermost), 10, 20, 30, 40, 50, 60, 70, 80, 90, 100 (outermost) mV/s on GCE. (B) The scan rate dependences for the Ru2 redox process at the LBL film with an outer POM layer.

currents for the Ru2 process plotted versus the scan rate. Thin layer behavior was clearly observed up to 100 mV/s with the film exhibiting diffusion controlled redox processes beyond this scan rate.

The effect of the solution pH upon the redox activity of the Ru-redox processes within the Ru_4POM while immobilized in the LBL assembly was studied (Figure 6A). It was observed that the film showed stable redox activity associated with Ru-centers within the POM in the pH range 2−5 based on LiCl and $LiCH_3COO$ buffer solutions. There was a cathodic shift for each Ru-centre with the increase in pH. The associated number of protons was found by plotting the dependence of the Ru2 formal potential versus pH as seen in Figure 6(B). The observed shift was 66 (±5) mV pH^{-1}, which is indicative of the involvement of one proton for this monoelectronic redox process.[35] Stability of the LBL assembly towards storage time was tested by storing the modified electrode in 0.1 HCl buffer for 18 h and cyclic voltammograms were recorded and

Table 2. Electrochemical Redox Properties of Ru_4POM in Solution and within a PDDA Modified GCE in 0.1 M HCl (vs Ag/AgCl)[a]

	E_{pa} (mV)		E_{pc} (mV)					
redox wave	soln.	layer	soln.	layer	$E_{1/2}$ mV soln.	$E_{1/2}$ mV monolayer	ΔE mV soln.	ΔE mV monolayer
Ru5	+1095	+1099	+1032	+1042	+1064	+1070	63	57
Ru4	+985	+895	+800	+871	+893	+883	185	24
Ru3	+666	+599	+605	+564	+636	+582	61	35
Ru2	+502	+460	+443	+444	+473	+452	59	16
Ru1	+306	+255	+145	+154	+226	+204	161	48

[a]Scan rate 50 mV/s.

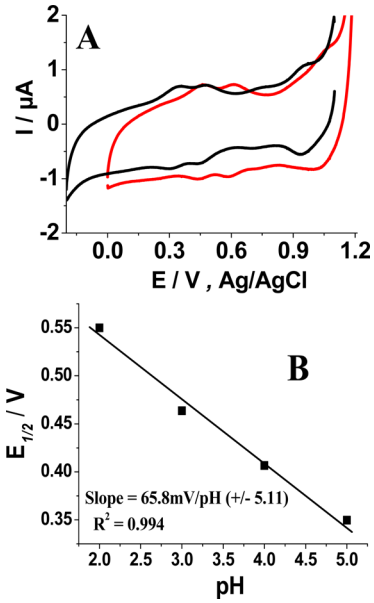

Figure 6. (A) Cyclic voltammograms 6 bilayers of LBL assembly of Ru_4POM-RuDend with outer POM layer in pH 2 (red) and pH 4 (black) scan rate 50 mV/s. (B) Dependence of formal potential on to the pH for the Ru2 redox process.

fingerprints of the Ru_4POM were still observed with some leaching of POM into the solution as shown in Supporting Information Figure S5.

3.3. Electrochemical Impedance Spectroscopy (EIS). Electrochemical impedence spectroscopy is a well developed technique to observe the kinetic and diffusion parameters of redox active species both in solution and on the surface of electrodes.[51] It has been used here during the various deposition steps of the LBL assembly whilst employing the Randles Circuit to aid in the interpretation of the resulting data,[52] where R_{CT} is the charge transfer resistance, R_s is the solution resistance, Z_W is the Warburg resistance and C_{dl} is the double layer capacitance. Figure 7A presents the Nyquist plot for the impedance spectra obtained during the construction of the Ru_4POM LBL assembly. Table 3 shows the resulting R_{CT} values obtained after the deposition of each layer within the multilayer assembly, which was roughly evaluated as a diameter of the semicircle at the kinetically controlled region. For the initial layers the $Fe(CN)_6^{3-/4-}$ redox process was diffusion controlled, however, with the further deposition of layers the $Fe(CN)_6^{3-/4-}$ redox process becomes kinetically controlled with a corresponding increase in the R_{CT} value, as can be seen in Table 3. This behavior is observed for other multilayer systems and is indicative of the increased pathway length to the electrode surface and reduced number of pathways for the redox probe.[52] In addition, non linear behavior was observed for the R_{CT} values after every deposition step indicating the differences in the film structure for the inner and outer layers.[52] Similar results were obtained for our system indicating the difference in the inner and outer layers of the film structure.

The permeability of the Ru_4POM based multilayer assemblies was investigated by studying the redox activity of both mono-electronic anionic and cationic redox probes, namely, $Fe(CN)_6^{3-}$ and $Ru(NH_3)_6^{2+}$, respectively. Parts B and C of Figures 7 show the redox activity of the $Fe(CN)_6^{3-}$ and $Ru(NH_3)_6^{2+}$ redox probes at a GCE modified with a Ru_4POM multilayer assembly composed of 6 bilayers with an outer POM layer, respectively. What is readily observed is that upon increasing layer number the redox activities of both probe molecules is only slightly reduced in magnitude. This implies that the resulting LBL layers are porous in nature as in agreement with the attained R_{CT} values in Table 3.

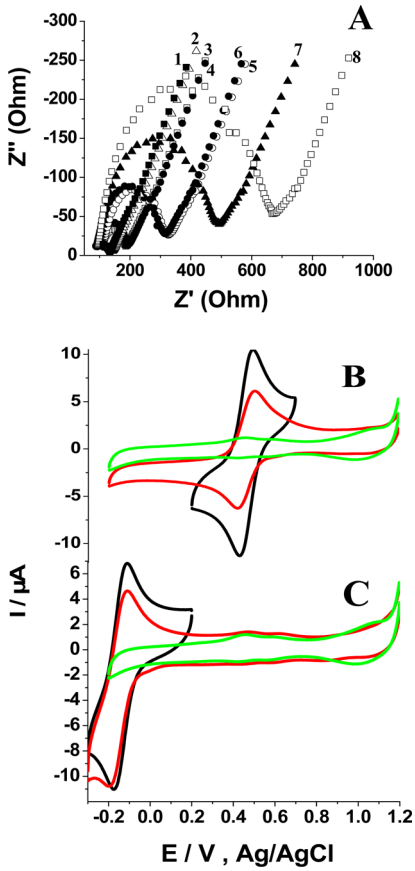

Figure 7. (A) Deposition steps of Ru_4POM-RuDend LBL film monitored by EIS, presented as Nyquist plot of impedance spectra of LBL modified electrode (■1, spectrum of blanck GCE; Δ2, spectrum of PDDA-modified electrode; □3, 1st Ru_4POM layer; ●4, 2nd RuDend layer; ○5, 3rd Ru_4POM layer; ●6, 4th RuDend layer; ▲7, 5th Ru_4POM layer; □8, 6th RuDend layer in 10 mM 1:1 ratio of $Fe(CN)_6^{3-/4-}$ in 0.1 M KCl; 10 mV amplitude, 230 mV potential of measurement. (B) Permeability of films by anionic redox probe, cyclic voltammograms were recorded at 0.1 M HCl before (green) and after (red) addition of 1 mM $K_3[Fe(CN)_6]$. CV at blank GCE (black). (C) Permeability of films by cationic redox probe, cyclic voltammograms were recorded at 0.1 M HCl buffer before (green) and after (red) addition of 1 mM $Ru(NH_3)_6Cl_2$. CV at blank GCE (black).

Table 3. Values of R_{CT} (Ω) for Each Monolayer and the Bare GCE[a]

layer no.	nature of layer	Ru_4POM R_{CT} (Ω)
substrate	bare glassy carbon electrode	14
1	PDDA	33
2	Ru_4POM	60
3	Ru-Dend	114
4	Ru_4POM	226
5	Ru-Dend	238
6	Ru_4POM	407

[a]The frequency range is 0.1 Hz to 10^5 Hz with signal amplitude of 5 mV. Initial potential: +230 mV. Electrolyte solution: 0.01 M $K_4[Fe(CN)_6]/K_3[Fe(CN)_6]$ (1:1) in 0.1 M KCl.

dx.doi.org/10.1021/am405295c | ACS Appl. Mater. Interfaces 2014, 6, 8022−8031

3.4. AFM, SEM, and XPS. Surface imaging along with the elemental analysis of the Ru_4POM LBL and polypyrrole films deposited on ITO-coated glass slides was performed by AFM, SEM, and XPS. Figure 8A shows the SEM image of the

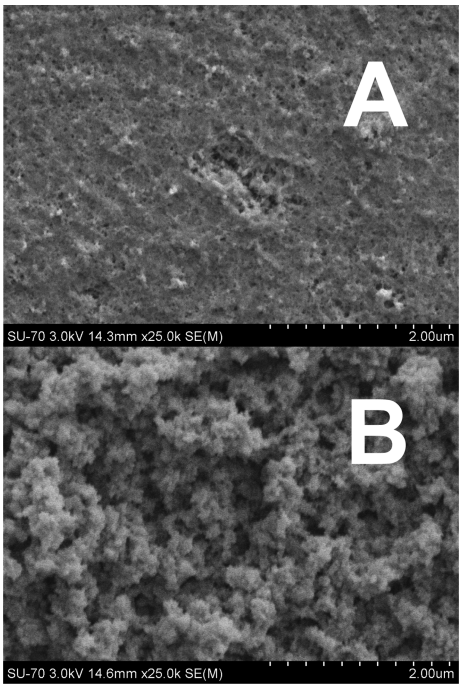

Figure 8. (A) SEM image of Ru_4POM doped polypyrrole film with deposition charge of 30mC grown from acetonitrile. (B) SEM image of Ru_4POM doped polypyrrole film with deposition charge of 30mC grown from water.

Ru_4POM doped polypyrrole film deposited from acetonitrile with a charge of 30mC. Pores of 10−20 nm and some surface cracks induced during drying were observed, but discrete particles could not be distinguished. Figure 8B shows the SEM image of the Ru_4POM doped polypyrrole film deposited from aqueous solution with a charge of 30 mC. This film appears to be thick in nature exhibited a globular morphology, with individual particles of 50−100 nm diameter clustered into agglomerates of approximately 600 nm diameter. C, N, O, Ru, and W were confirmed to be present by EDS, which indicated the presence of Ru_4POM in both films; these results were consistent with the XPS data presented.

The presence of polypyrrole was confirmed from the high resolution N 1s and C 1s XPS spectra. The N 1s spectra can be decomposed mainly into 2 component peaks. The lower binding energy peak at 399.6 eV was attributed to neutral nitrogen in polypyrrole and the peak at 401.1 eV was attributed to protonated nitrogen. The related carbon peak representing C−N of the polypyrrolic chains appears at 286.3 eV in the carbon spectrum. The ratio of $N^+/N(total)$ for the Ru_4POM doped polymer is 0.32, which gives an estimate of the polymer's doping level. The presence of the Ru_4POM is also confirmed by the W, Ru, and Si signals in the XPS spectrum. Analysis of the Ru_4POM-$[RuDend]^{8+}$ based LBL film, showed the presence of N (5.7 %), C (49.3%), O (36.2%), W (5.9%), Si (0.9%), and Ru (2%). Figure 9A and B shows the presence of W in the XPS spectra of the LBL and polymeric films, respectively. Full spectra of XPS data for the LBL assemblies and polypyrrole

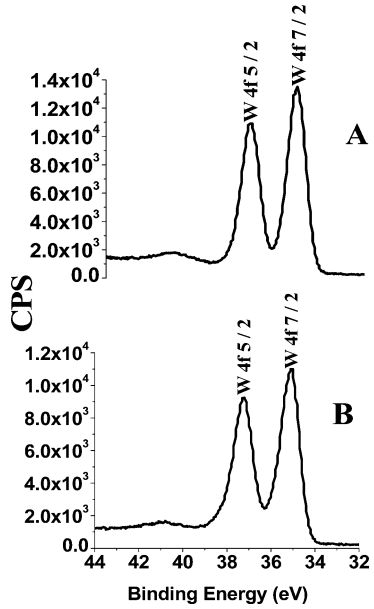

Figure 9. (A) XPS spectrum of 11 bilayers of Ru_4POM-RuDend multilayer assembly showing tungsten. (B) XPS spectrum of Ru_4POM doped polypyrrole film with deposition charge of 30 mC grown from acetonitrile showing tungsten.

films are shown in Supporting Information Figure S7, A and B, respectively.

AFM imaging was conducted at intervals throughout the multilayer deposition process to examine variations in the topography during the process. The samples imaged were as follows: blank ITO slide, ITO/PDDA, ITO/PDDA/Ru_4POM, and ITO/PDDA/Ru_4POM(RuDend-$Ru_4POM)_6$ LBL assembly to find the topography of the multilayers. The values of root mean square surface roughness (S_q) for these layers were 18.9 nm, 19.4, 1.93, and 4.59 nm, respectively. Particles of widely varying sizes, up to ~1μm in diameter, were observed on the blank ITO surface, consistent with the SEM findings. The largest of these features remained visible in the AFM images obtained from PDDA modified ITO, along with a more globular structure indicative of a polymeric film. Further variations in surface topography were observed during deposition of the multilayer film, as shown in Figure 10A. The topography observed for the Ru_4POM doped polypyrrole film is shown in Figure 10B. Topographic images of blank ITO, PDDA modified ITO and monolayer of Ru_4POM onto PDDA modified ITO slides have been presented in Supporting Information Figure S8, A, B, and C respectively. The topographies of both the LBL assembly and Ru_4POM doped polymeric films featured globular structures. Significantly varied diameter of these globules was observed within the same sample and between samples. These structures had an overall hemispherical shape, which may be most readily seen in the topographic images. The globule sizes and S_q values observed for of Ru_4POM doped polypyrrole films were two orders of magnitude larger than those observed for the corresponding LBL film. Little phase contrast was seen for all the films analysed. This suggested that the samples consisted of a homogenous surface within the areas of interest imaged, in keeping with the EDS and XPS analyses. These findings are consistent with previous studies of analogous multilayer systems and polymeric systems.[48,53]

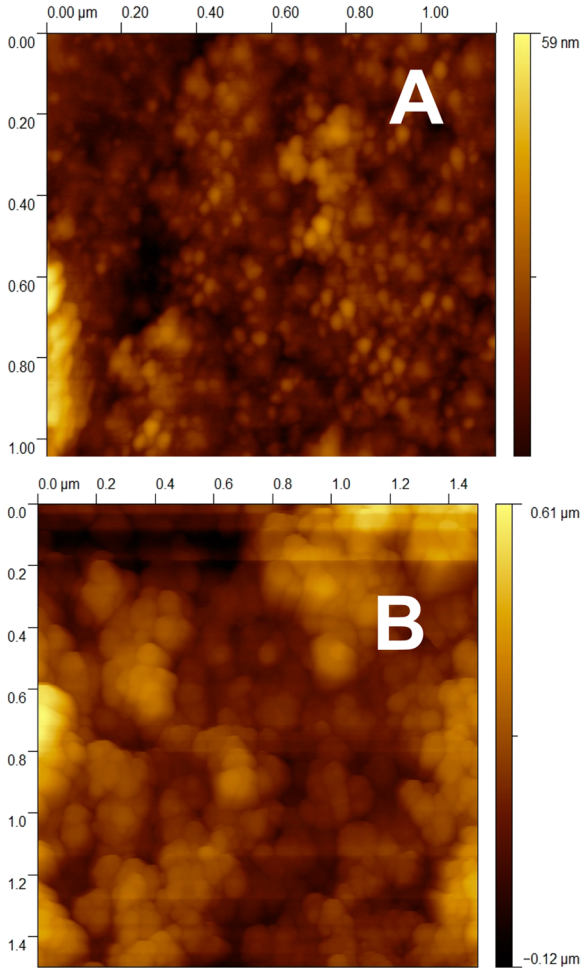

Figure 10. (A) AFM image of 6 bilayers of Ru_4POM-RuDend multilayer assembly. (B) AFM image of Ru_4POM doped polypyrrole film with deposition charge of 30 mC grown from acetonitrile.

3.5. Preliminary Results of Water Oxidation Catalysis.

The electrocatalytic activity of Ru_4POM towards the oxidation of water has been previously reported both in solution, with $Ru(bpy)_3^{2+}$ as the electron transfer mediator, and in the heterogeneous phase when supported on carbon nanostructured materials.[29,44] Preliminary investigations in the ability of the LBL assembly towards the electrocatalytic oxidation of water have been undertaken in aerated PBS pH7 buffer at a scan rate 25 mV/s. The redox behavior of the LBL assembly was investigated between pH 2 and 5, since in this pH range the POM exhibits clearly defined redox waves. The catalytic activity was investigated at neutral pH 7 as it closely matches the conditions for a possible future application, with the catalysis at pH 7 being undertaken previously.[32−34] For comparison the paste of Ru_4POM was also tested under similar conditions towards the electro-oxidation of water as can be seen in Figure 11 where the black trace represents the LBL assembly and the red trace indicates the paste of Ru_4POM. In the LBL assembly an oxidation wave commences at +0.8 V (vs Ag/AgCl) with the onset of water oxidation at +1.07 V, where as the paste shows the oxidation wave at +0.9 V with the onset of water oxidation at +1.1 V, with similar overpotentials being observed for other systems where the Ru_4POM was anchored onto nanostructured carbon based materials[44] or confined within highly porous wet graphene films.[38] In addition, the

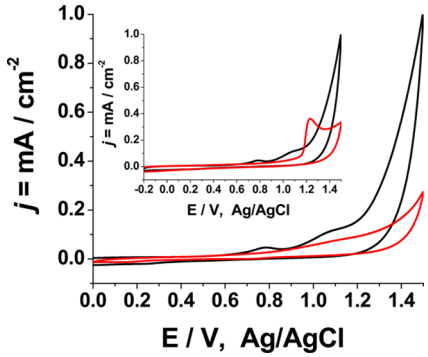

Figure 11. Resulting current density curves for the electrocatalytic oxidation of water in pH7 PBS buffer with the Ru_4POM paste (red) and Ru_4POM-$[RuDend]^{8+}$ 6 bilayer assembly (black) on a GCE, scan rate 25 mV/s. Inset shows the cyclic voltammogram of 6 bilayers (black) of an Ru_4POM-$[RuDend]^{8+}$ LBL assembly and 6 bilayers (red) of a $K_8[P_2W_{18}O_{62}]$-$[RuDend]^{8+}$ LBL assembly in pH7 PBS buffer at GCE, scan rate 25 mV/s.

multilayer assembly showed the higher oxidation current as compared to the paste of the POM, thus proving the better performance of the Ru_4POM in LBL assembly with $[RuDend]^{8+}$ for the electro-oxidation of water. The inset of Figure 11 shows the cyclic voltammogrames of LBL assemblies of 6 bilayers of Ru_4POM- $[RuDend]^{8+}$ (black trace) and 6 bilayers of $K_8[P_2W_{18}O_{62}]$ POM- $[RuDend]^{8+}$ (red trace), prepared in an analogous method as to the Ru_4POM-$[RuDend]^{8+}$ LbL assembly, by using a Ruthenium free POM supposed to be inert in water oxidation catalysis, in PBS solution of pH7. Indeed, in this latter case only the oxidation of the [RuDend] moiety is observed, at E = 1.2 V vs Ag/AgCl; although this process is likely to occur also in the case of the Ru_4POM-$[RuDend]^{8+}$ LbL assembly, the high intensity of the current speaks in favor of an electrocatalytic process involving water oxidation. O_2 evolution was confirmed by the presence of a cathodic wave (E = −0.50 V vs Ag/AgCl) observed only in the reverse scan, due to reduction of dioxygen formed at the working electrode (Figure S10 in the Supporting Information) with the LBL assembly of 6 bilayers of Ru_4POM-$[RuDend]^{8+}$. The attribution of this cathodic wave to reduction of dioxygen was indeed confirmed by registering the cyclic voltammogram upon air bubbling into the solution. Stability of the modified electrode was tested by recording the cyclic voltammogram before and after the catalysis. The redox activity associated with the Ru_4POM was apparent, as can be seen in Supporting Information Figure S6. Major leaching of the Ru_4POM from the LbL is observed, as confirmed by CV scans on the electrode after catalysis (Supporting Information Figure S6), and by the marked abatement of the resonant Raman signals (250−500 cm^{-1}) (Supporting Information Figure S9).

4. CONCLUSIONS

$[\{Ru_4O_4(OH)_2(H_2O)_4\}(\gamma\text{-}SiW_{10}O_{36})_2]^{10-}$ POM with organic and inorganic cationic parts has been successfully immobilised onto GCE and ITO coated glass slides using conducting polypyrrole films and the LBL assembly technique employing a Ru(II)-metallodendrimer as the cationic moiety for the LBL films. Stable and reproducible films were produced by both methods, which showed stability in pH range 2−5 for the POM based redox couples. Polymeric films exhibited thin layer behavior up to 1 V/s whilst the LBL assembly exhibited thin layer behavior only up to 100 mV/s. The surface morphology

dx.doi.org/10.1021/am405295c | ACS Appl. Mater. Interfaces 2014, 6, 8022−8031

of the polymeric and LBL films was comparable to that reported for analogous systems in the literature. The LBL assemblies were found to be quite porous with good permeability towards the redox probes. The Ru_4POM based LBL assemblies exhibited enhanced electrocatalytic abilities towards water oxidation in pH7 PBS buffer, in comparison to both Ru_4POM paste electrodes and LBL assemblies composed of the Dawson Parent POM moiety, $K_8[P_2W_{18}O_{62}]$.

■ ASSOCIATED CONTENT

Supporting Information

Structure of the Ru-metallodendrimer $[RuDend]^{8+}$, schematic presentation of the Ru_4POM-$[Ru\text{-}Dend]^{8+}$ based LBL films, Ru_4POM doped polypyrrole films grown from acetonitrile and aqueous media, stability of the polypyrrole film towards the redox cycling, cyclic voltammograms of LBL assembly showing stability after storage time, after catalysis, full XPS spectrum of 11 bilayers of LBL assembly, full XPS spectrum of polypyrrole films, AFM images of different deposition steps of multilayer assembly, raman spectra of polypyrrole films and LBL assembly before and after catalysis and cyclic voltammogram showing O_2 confirmation. This material is available free of charge via the Internet at http://pubs.acs.org/.

■ AUTHOR INFORMATION

Corresponding Author

*Fax: +353 42 933 1163. Tel: +353 42 937 4579. Email: tim.mccormac@dkit.ie.

Notes

The authors declare no competing financial interest.

■ ACKNOWLEDGMENTS

AFM, SEM, and XPS experiments were conducted under the framework of the INSPIRE programme, funded by the Irish Government's Programme for Research in Third Level Institutions, Cycle 4, National Development Plan 2007–2013. The EU-COST Action CM1203 Polyoxometalate Chemistry for Molecular Nanoscience – PoCheMoN is gratefully acknowledged. We thank Dr. Zois Syrgiannis (University of Trieste, Italy) for undertaking resonance Raman spectroscopy.

■ REFERENCES

(1) Muradov, N.; T-Raissi, A. Solar Production of Hydrogen Using "Self-Assembled" Polyoxometalate Photocatalysts. *J. Sol. Energy Eng.* **2006**, *128*, 326–331.

(2) Xu, W.; Liu, C.; Xing, W.; Lu, T. A Novel Hybrid based on Carbon Nanotubes and Heteropolyanions as Effective Catalyst for Hydrogen Evolution. *Electrochem. Commun.* **2007**, *9*, 180–184.

(3) Ni, M.; Leung, M. K. H.; Leung, D. Y. C.; Sumathy, K. A Review and Recent Developments in Photocatalytic Water-Splitting using TiO_2 for Hydrogen Production. *Renewable Sustainable Energy Rev.* **2007**, *11*, 401–425.

(4) Kuznetsov, A. E.; Geletii, Y. V.; Hill, C. L.; Morokuma, K.; Musaev, D. G. Dioxygen and Water Activation Processes on Multi-Ru-Substituted Polyoxometalates: Comparison with the "Blue-Dimer" Water Oxidation Catalyst. *J. Am. Chem. Soc.* **2009**, *131*, 6844–6854.

(5) Geletii, Y. V.; Huang, Z.; Hou, Y.; Musaev, D. G.; Lian, T.; Hill, C. L. Homogeneous Light-Driven Water Oxidation Catalyzed by a Tetraruthenium Complex with All Inorganic Ligands. *J. Am. Chem. Soc.* **2009**, *131*, 7522–7523.

(6) Puntoriero, F.; Sartorel, A.; Orlandi, M.; La Ganga, G.; Serroni, S.; Bonchio, M.; Scandola, F.; Campagna, S. Photoinduced Water Oxidation using Dendrimeric Ru(II) Complexes as Photosensitizers. *Coord. Chem. Rev.* **2011**, *255*, 2594–2601.

(7) Umena, Y.; Kawakami, K.; Shen, J.-R.; Kamiya, N. Crystal Structure of Oxygen-Evolving Photosystem II at a Resolution of 1.9 Å. *Nature* **2011**, *473*, 55–60.

(8) McEvoy, J. P.; Brudvig, G. W. Water-Splitting Chemistry of Photosystem II. *Chem. Rev.* **2006**, *106*, 4455–4483.

(9) Huynh, M. H. V.; Meyer, T. J. Proton-Coupled Electron Transfer. *Chem. Rev.* **2007**, *107*, 5004–5064.

(10) Meyer, T. J.; Huynh, M. H. V.; Thorp, H. H. The Possible Role of Proton-Coupled Electron Transfer (PCET) in Water Oxidation by Photosystem II. *Angew. Chem. Int. Ed.* **2007**, *46*, 5284–5304.

(11) Dau, H.; Haumann, M. The Manganese Complex of Photosystem II in its Reaction Cycle—Basic Framework and Possible Realization at the Atomic Level. *Coord. Chem. Rev.* **2008**, *252*, 273–295.

(12) Gersten, S. W.; Samuels, G. J.; Meyer, T. J. J. Catalytic Oxidation of Water by an Oxo-Bridged Ruthenium Dimer. *J. Am. Chem. Soc.* **1982**, *104*, 4029–4030.

(13) Moonshiram, D.; Jurss, J. W.; Concepcion, J. J.; Zakharova, T.; Alperovich, I.; Meyer, T. J.; Pushkar, Y. Structure and Electronic Configurations of the Intermediates of Water Oxidation in Blue Ruthenium Dimer Catalysis. *J. Am. Chem. Soc.* **2012**, *134*, 4625–4636.

(14) Jurss, J. W.; Concepcion, J. C.; Norris, M. R.; Templeton, J. L.; Meyer, T. J. Surface Catalysis of Water Oxidation by the Blue Ruthenium Dimer. *Inorg. Chem.* **2010**, *49*, 3980–3982.

(15) Deng, Z.; Tseng, H.-W.; Zong, R.; Wang, D.; Thummel, R. Preparation and Study of a Family of Dinuclear Ru(II) Complexes that Catalyze the Decomposition of Water. *Inorg. Chem.* **2008**, *47*, 1835–1848.

(16) Wada, T.; Tsuge, K.; Tanaka, K. Syntheses and Redox Properties of Bis(hydroxoruthenium) Complexes with Quinone and Bipyridine Ligands. Water-Oxidation Catalysis. *Inorg. Chem.* **2000**, *40*, 329–337.

(17) Sens, C.; Romero, I.; Rodríguez, M.; Llobet, A.; Parella, T.; Benet-Buchholz, J. A New Ru Complex Capable of Catalytically Oxidizing Water to Molecular Dioxygen. *J. Am. Chem. Soc.* **2004**, *126*, 7798–7799.

(18) Xu, Y.; Duan, L.; Tong, L.; Akermark, B.; Sun, L. Visible Light-Driven Water Oxidation Catalyzed by a Highly Efficient Dinuclear Ruthenium Complex. *Chem. Commun.* **2010**, *46*, 6506–6508.

(19) Duan, L. L.; Bozoglian, F.; Mandal, S.; Stewart, B.; Privalov, T.; Llobet, A.; Sun, L. C. A Molecular Ruthenium Catalyst with Water-Oxidation Activity Comparable to that of Photosystem II. *Nat. Chem.* **2012**, *4*, 418–423.

(20) Duan, L.; Xu, Y.; Zhang, P.; Wang, M.; Sun, L. Visible Light-Driven Water Oxidation by a Molecular Ruthenium Catalyst in Homogeneous System. *Inorg. Chem.* **2009**, *49*, 209–215.

(21) Bozoglian, F.; Romain, S.; Ertem, M. Z.; Todorova, T. K.; Sens, C.; Mola, J.; Rodríguez, M.; Romero, I.; Benet-Buchholz, J.; Fontrodona, X.; Cramer, C. J.; Gagliardi, L.; Llobet, A. The Ru-Hbpp Water Oxidation Catalyst. *J. Am. Chem. Soc.* **2009**, *131*, 15176–15187.

(22) Xu, Y.; Fischer, A.; Duan, L.; Tong, L.; Gabrielsson, E.; Åkermark, B.; Sun, L. Chemical and Light-Driven Oxidation of Water Catalyzed by an Efficient Dinuclear Ruthenium Complex. *Angew. Chem. Int. Ed.* **2010**, *49*, 8934–8937.

(23) Sartorel, A.; Carraro, M.; Scorrano, G.; Zorzi, R. D.; Geremia, S.; McDaniel, N. D.; Bernhard, S.; Bonchio, M. Polyoxometalate Embedding of a Tetraruthenium(IV)-Oxo-Core by Template-Directed Metalation of $[\gamma\text{-}SiW_{10}O_{36}]^{8-}$. A totally Inorganic Oxygen-Evolving Catalyst. *J. Am. Chem. Soc.* **2008**, *130*, 5006–5007.

(24) Pope, M. T. *Heteropoly and Isopoly Oxometalates*; Springer-Verlag: New York, 1983.

(25) Pope, M. T.; Müller, A. Polyoxometalate Chemistry—An Old Field with New Dimensions in Several Disciplines. *Angew. Chem. Int. Ed.* **1991**, *30*, 34–48.

(26) Pope, M. T.; Müller, A. *Polyoxometalates: From Platonic Solids to Anti-retroviral Activity*; Kluwer Academic Publishers: Dordrecht, The Netherlands, 1994.

(27) Vickers, J. W.; Lv, H.; Sumliner, J. M.; Zhu, G.; Luo, Z.; Musaev, D. G.; Geletii, Y. V.; Hill, C. L. Differentiating Homogeneous and Heterogeneous Water Oxidation Catalysis: Confirmation that $[Co_4(H_2O)_2(\alpha\text{-}PW_9O_{34})_2]^{10-}$ is a Molecular Water Oxidation Catalyst. *J. Am. Chem. Soc.* **2013**, *135*, 14110−14118.
(28) Song, F.; Ding, Y.; Ma, B.; Wang, C.; Wang, Q.; Du, X.; Fu, S.; Song, J. $K_7[CoIIICoII(H_2O)W_{11}O_{39}]$: A Molecular Mixed-Valence Keggin Polyoxometalate Catalyst of High Stability and Efficiency for Visible Light-Driven Water Oxidation. *Energy Environ. Sci.* **2013**, *6*, 1170−1184.
(29) Geletii, Y. V.; Botar, B.; Kögerler, P.; Hillesheim, D. A.; Musaev, D. G.; Hill, C. L. An All-Inorganic, Stable, and Highly Active Tetraruthenium Homogeneous Catalyst for Water Oxidation. *Angew. Chem. Int. Ed.* **2008**, *47*, 3896−3899.
(30) Liu, Y. P.; Guo, S. X.; Bond, A. M.; Zhang, J.; Geletii, Y. V.; Hill, C. L. Voltammetric Determination of the Reversible Potentials for $[\{Ru_4O_4(OH)_2(H2O)_4\}(\gamma\text{-}SiW_{10}O_{36})_2]^{10-}$ Over the pH Range 2−12: Electrolyte Dependence and Implications for Water Oxidation Catalysis. *Inorg. Chem.* **2013**, *52*, 11986−11996.
(31) Natali, M.; Orlandi, M.; Berardi, S.; Campagna, S.; Bonchio, M.; Sartorel, A.; Scandola, F. Photoinduced Water Oxidation by a Tetraruthenium Polyoxometalate Catalyst: Ion-Pairing and Primary Processes With $Ru(bpy)_3^{2+}$ Photosensitizer. *Inorg. Chem.* **2012**, *51*, 7324−7331.
(32) Toma, F. M.; Sartorel, A.; Iurlo, M.; Carraro, M.; Parisse, P.; Maccato, C.; Rapino, S.; Rodriguez Gonzalez, B.; Amenitsch, H.; Da Ros, T.; Casalis, L.; Goldoni, A.; Marcaccio, M.; Scorrano, G.; Scoles, G.; Paolucci, F.; Prato, M.; Bonchio, M. Efficient Water Oxidation at Carbon Nanotube−Polyoxometalate Electrocatalytic Interfaces. *Nat. Chem.* **2010**, *2*, 826−831.
(33) Toma, F. M.; Sartorel, A.; Iurlo, M.; Carraro, M.; Rapino, S.; Hoober-Burkhardt, L.; Da Ros, T.; Marcaccio, M.; Scorrano, G.; Paolucci, F.; Bonchio, M.; Prato, M. Tailored Functionalization of Carbon Nanotubes for Electrocatalytic Water Splitting and Sustainable Energy Applications. *ChemSusChem* **2011**, *4*, 1447−1451.
(34) Quintana, M.; Lopez, A. M.; Rapino, S.; Toma, F. M.; Iurlo, M.; Carraro, M.; Sartorel, A.; Maccato, C.; Ke, X. X.; Bittencourt, C.; Da Ros, T.; Van Tendeloo, G.; Marcaccio, M.; Paolucci, F.; Prato, M.; Bonchio, M. Knitting the Catalytic Pattern of Artificial Photosynthesis to a Hybrid Graphene Nanotexture. *ACS Nano* **2013**, *7*, 811−817.
(35) Lee, C.-Y.; Guo, S.-X.; Murphy, A. F.; McCormac, T.; Zhang, J.; Bond, A. M.; Zhu, G.; Hill, C. L.; Geletii, Y. V. Detailed Electrochemical Studies of the Tetraruthenium Polyoxometalate Water Oxidation Catalyst in Acidic Media: Identification of an Extended Oxidation Series Using Fourier Transformed Alternating Current Voltammetry. *Inorg. Chem.* **2012**, *51*, 11521−11532.
(36) Sartorel, A.; Miroì, P.; Salvadori, E.; Romain, S.; Carraro, M.; Scorrano, G.; Valentin, M. D.; Llobet, A.; Bo, C.; Bonchio, M. Water Oxidation at a Tetraruthenate Core Stabilized by Polyoxometalate Ligands: Experimental and Computational Evidence to Trace the Competent Intermediates. *J. Am. Chem. Soc.* **2009**, *131*, 16051−16053.
(37) Geletii, Y. V.; Besson, C.; Hou, Y.; Yin, Q.; Musaev, D. G.; Quiñonero, D.; Cao, R.; Hardcastle, K. I.; Proust, A.; Kögerler, P.; Hill, C. L. Structural, Physicochemical, and Reactivity Properties of an All-Inorganic, Highly Active Tetraruthenium Homogeneous Catalyst for Water Oxidation. *J. Am. Chem. Soc.* **2009**, *131*, 17360−17370.
(38) Guo, S. X.; Liu, Y. P.; Lee, C. Y.; Bond, A. M.; Zhang, J.; Geletiib, Y. V.; Hill, C. L. Graphene-Supported $[\{Ru_4O_4(OH)_2(H_2O)_4\}(\gamma\text{-}SiW_{10}O_{36})_2]^{10-}$ for Highly Efficient Electrocatalytic Water Oxidation. *Energy Environ. Sci.* **2013**, *6*, 2654−2663.
(39) Sala, X.; Romero, I.; Rodríguez, M.; Escriche, L.; Llobet, A. Molecular Catalysts That Oxidize Water to Dioxygen. *Angew. Chem. Int. Ed.* **2009**, *48*, 2842−2852.
(40) Natali, M.; Berardi, S.; Sartorel, A.; Bonchio, M.; Campagna, S.; Scandola, F. Is $[Co_4(H_2O)_2(\boldsymbol{\alpha}\text{-}PW_9O_{34})_2]^{10-}$ a Genuine Molecular Catalyst in Photochemical Water Oxidation. *Chem. Commun.* **2012**, *48*, 8808−8810.
(41) Stracke, J. J.; Finke, R. G. Water Oxidation Catalysis Beginning with $Co_4(H_2O)_2(PW_9O_{34})_2^{10-}$ When Driven by the Chemical Oxidant Ruthenium(III)tris(2,2′-bipyridine): Stoichiometry, Kinetic, and Mechanistic Studies En Route to Identifying the True Catalyst. *ACS Catal.* **2013**, *4*, 79−85.
(42) Qiu, J. B.; Villemure, G. J. Anionic Clay-Modified Electrodes—Electrochemical Activity of Nickel(II) Sites in layered Double Hydroxide Films. *Electroanal. Chem.* **1995**, *395*, 159−166.
(43) He, J. X.; Kobayashi, K.; Takahashi, M.; Villemure, G.; Yamagishi, A. Preparation of Hybrid Films of an Anionic Ru(II) Cyanide Polypyridyl Complex With Layered Double Hydroxides by the Langmuir-Blodgett Method and Their use as Electrode Modifiers. *Thin Solid Films* **2001**, *397*, 255−265.
(44) Toma, F. M.; Sartorel, A.; Carraro, M.; Bonchio, M.; Prato, M. Dendron-Functionalized Multiwalled Carbon Nanotubes Incorporating Polyoxometalates for Water-Splitting Catalysis. *J. Pure Appl. Chem.* **2011**, *83*, 1529−1542.
(45) Ma, H.; Shi, S.; Zhang, Z.; Pang, H.; Zhang, Y. J. A Thin Film of the Di-decatungstosilicate with a Tetra-Ruthenium(IV)-Oxo Core and Its Electrochemical Properties. *Electroanal. Chem.* **2010**, *648*, 128−133.
(46) Constable, C. E.; Housecroft, E. C.; Cattalini, M.; Phillips, D. Pentaerythritol-Based Metallodendrimers. *New J. Chem.* **1998**, *22*, 193−200.
(47) McCormac, T.; Farrell, D.; Drennan, D.; Bidan, G. Immobilization of a Series of Dawson Type Heteropolyanions. *Electroanalysis* **2001**, *13*, 836−842.
(48) Anwar, N.; Vagin, M.; Naseer, R.; Imar, S.; Ibrahim, M.; Mal, S. S.; Kortz, U.; Laffir, F.; McCormac, T. Redox Switching of Polyoxometalate-Methylene Blue-Based Layer-by-Layer Films. *Langmuir* **2012**, *28*, 5480−5488.
(49) Weinberg, D. R.; Gagliardi, C. J.; Hull, J. F.; Murphy, C. F.; Kent, C. A.; Westlake, B. C.; Paul, A.; Ess, D. H.; McCafferty, D. G.; Meyer, T. J. Proton-Coupled Electron Transfer. *Chem. Rev.* **2012**, *112*, 4016−4093.
(50) Liu, F.; Concepcion, J. J.; Jurss, J. W.; Cardolaccia, T.; Templeton, J. L.; Meyer, T. J. Mechanisms of Water Oxidation from the Blue Dimer to Photosystem II. *Inorg. Chem.* **2008**, *47*, 1727−1752.
(51) Bard, A. J.; Faulkner, L. R. *Electrochemical Methods: Fundamentals and Applications*, 2nd ed.; John Wiley & Sons, Inc: New York, 2001.
(52) Harris, J. J.; Bruening, M. L. Electrochemical and In Situ Ellipsometric Investigation of the Permeability and Stability of Layered Polyelectrolyte Films. *Langmuir* **2000**, *16*, 2006−2013.
(53) Zynek, M.; Serantoni, M.; Beloshapkin, S.; Dempsey, E.; McCormac, T. Electrochemical and Surface Properties of Multilayer Films Based on a Ru^{8+} Metallodendrimer and the Mixed Addenda Dawson Heteropolyanion. *Electroanalysis* **2007**, *19*, 681−689.